9

Sea-ice modelling

GREGORY M. FLATO
Canadian Centre for Climate Modelling and Analysis,
Meteorological Service of Canada

Representing the mass balance of sea ice involves solving a coupled, non-linear set of equations describing ice motion (momentum balance), thermodynamic growth and melt (energy balance) and the transport and redistribution of ice thickness (area and volume conservation). A detailed description of the theory underlying sea-ice models is provided in Chapter 7, and so only a brief review is provided here. It is the case that approximations employed to represent many important processes, both in stand-alone ice models and in more comprehensive global climate models, lead to errors or uncertainties in simulated sea-ice behaviour. Nonetheless, because of the scarcity of direct observations related to sea-ice mass balance, models provide valuable insight into the mean state of the ice cover and its historical and projected future changes.

9.1 Brief overview of sea-ice models

The sea-ice mass balance involves local growth and melt, horizontal transport and deformation. These processes alter the local mean thickness (ice volume per unit area) and involve exchanges of mass (fresh water) and energy with the atmosphere and ocean. Figure 9.1 provides an illustration, for the Arctic, based on results of a stand-alone sea-ice model (Hilmer, Harder and Lemke, 1998). In this figure the annual mean ice transport is indicated by the vectors, the annual mean ice thickness by the solid contours and the net freezing rate (net ice growth minus ice melt – directly proportional to the salt flux delivered to the ocean surface) by the coloured shading. The general pattern is anticyclonic circulation within the Arctic basin and outflow of ice through the Fram Strait that is balanced by net ice growth over much of the basin. The mean transport pattern leads to convergent deformation and thickening along the Canadian Arctic islands and Greenland, with divergence and correspondingly thin ice along the central Eurasian coast. For Antarctica, the pattern (not shown)
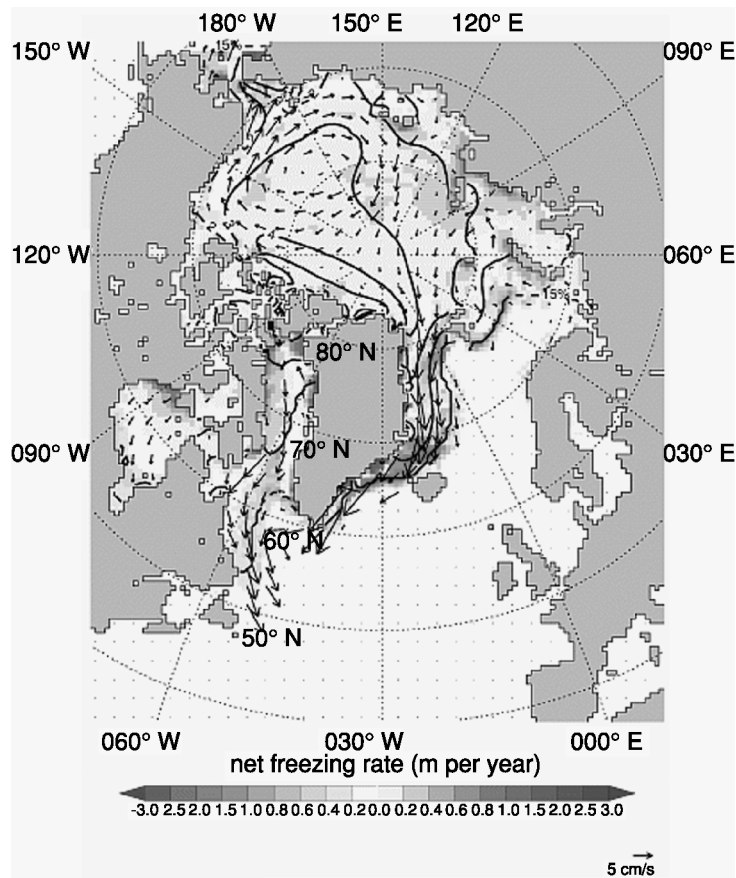
Figure 9.1. Components of the Arctic sea-ice mass balance. Vectors show annual mean ice transport; the solid contours (contour interval of 1 m) show annual mean ice thickness; and the coloured shading indicates net freezing rate (net ice growth minus melt – positive values correspond to a net salt flux to the ocean). (Figure provided by M. Hilmer; Hilmer *et al.* (1998).)

is one of net divergence, and hence net ice growth, around much of the continent (with net melt further out in the Southern Ocean), and rather thinner ice in general.

Representing features of the sort illustrated in Figure 9.1 in either a stand-alone sea-ice model or in a global climate model involves the following:

- solution of a momentum equation to obtain the ice velocity field;
- solution of a thermodynamic equation to obtain net ice growth or melt;
- solution of conservation equations that includes ice transport and deformation along with the thermodynamic sources and sinks.

These model components will be discussed briefly in turn. More comprehensive reviews are available in Chapter 7, Fichefet, Goosse and Morales Maqueda (1998), Hibler (1986), Hibler and Flato (1992) and Steele and Flato (2000).

9.1.1 Momentum equation

The balance of horizontal forces on a parcel of ice may be represented as

$$\rho_i h \frac{\partial u}{\partial t} = -\rho_i h \mathbf{k} \times \mathbf{u} + \boldsymbol{\tau}_a + \boldsymbol{\tau}_o - \rho_i g h \nabla \eta + \nabla \cdot \boldsymbol{\sigma}, \qquad (9.1)$$

where ρ_i is the ice density, h is the mean thickness (ice volume per unit area), $\mathbf{u}$ is the ice velocity vector, t is time, $\mathbf{k}$ is a unit vertical vector, $\boldsymbol{\tau}_a$ is the wind stress applied on the ice surface, $\boldsymbol{\tau}_o$ is the ocean stress applied on the ice underside, g is the acceleration due to gravity, η is the ocean surface elevation and $\boldsymbol{\sigma}$ is the internal ice stress tensor (a non-linear function of the ice state and strain or strain rate). Note that in this equation the non-linear momentum advection term has been neglected (on the basis of a scaling argument). In addition, the ice is considered to behave as a two-dimensional continuum. This assumption is harder to justify, especially at spatial scales of tens of kilometres or less where pack ice behaves more as a collection of semi-rigid 'floes' or 'plates' (e.g. Moritz and Stern, 2001; Moritz and Ukita, 2000; Thorndike, 1987); however, as in soil mechanics, the continuum assumption is plausible at scales much larger than a typical ice floe, which is the case for the numerical grids employed by most of the models whose results will be discussed here.

The acceleration term on the left hand side of equation (9.1) is typically negligible for timescales longer than a few hours. It is, of course, crucial if one wishes to resolve the inertial oscillations apparent in high frequency ice motion, especially in the Antarctic (e.g. Geiger, Hibley and Ackley, 1998). Heil and Hibler (2002) describe a modification to equation (9.1) to account for the 'added mass' of the upper ocean in these oscillations, but this has not been included in the large-scale models considered here. In some circumstances, the deformation associated with inertial oscillations may contribute to the sea-ice mass balance (via additional opening and rafting/ridging), but this contribution is likely to be small at the basin scale.

The first three terms on the right hand side of equation (9.1) are the Coriolis force and the body forces due to wind drag on the upper surface and water drag on the ice underside. These latter terms are typically represented by a bulk boundary layer parameterization. The fourth term is the (generally small) force associated with tilt of the sea surface.

The last term in equation (9.1) is the force arising from gradients in the internal ice stress field; that is, the force resulting from the resistance of sea ice to deformation. This term poses one of the main challenges in sea-ice modelling. In general, the stress state depends on the ice state (e.g. thicker ice is stronger and so able to support larger stresses than thin ice) and on the extent to which the ice is being deformed. The relation between stress and strain or strain rate is termed 'rheology', and there have been several rheologies used in sea-ice modelling.

Early efforts represented the ice as a linear viscous fluid wherein stress is linearly dependent on strain rate (e.g. Campbell, 1965; Hibler, 1974); however such an approximation fails to reproduce the differences in deformation between the central pack and the near-shore regions. An elastic–plastic rheology (in which the stress depends linearly on strain until it reaches a specified failure or 'yield' strength) was proposed by Pritchard (1975) and used successfully by Pritchard, Coon and McPhee (1977) in a short-term, regional application. The necessity of resolving elastic waves and employing a Lagrangian grid renders the elastic–plastic scheme somewhat undesirable for long-term climate studies, although some of these shortcomings have been addressed recently (Polyakov *et al.*, 1998). The viscous–plastic model, introduced by Hibler (1979), grew out of these earlier attempts. Like the elastic–plastic rheology, it requires a specification of the plastic yield strength which, for mathematical convenience, was represented by an elliptical yield curve (see Hibler (1979) for a definition and further details). The difference is that pre-yield stress states are assumed to be linearly related to strain rate, as in the viscous rheology. It should be noted that there is no implication that sea ice behaves as a viscous fluid – indeed the pre-yield viscosities are somewhat arbitrary and are chosen in practice so that non-yielding ice is 'nearly rigid' (much as in the elastic–plastic case). The advantage of the viscous closure is that it permits an efficient numerical scheme well suited to large-scale, long-term simulations. The recent 'elastic–viscous–plastic' scheme of Hunke and Dukowicz (1997) is a variation on Hibler's scheme, and, while not really a different rheology (the elastic term is added strictly as a numerical artifice to allow an alternative and more efficient time-stepping scheme), it is an approach that is becoming widely used. Other authors have explored alternative yield formulations (alternative yield curve shapes or assumptions regarding the relative orientation of stress and strain rate vectors – the so-called 'flow rule'). Examples here include the cavitating fluid rheology and its extension to a Mohr–Coulomb triangular yield curve (Flato and Hibler, 1992), and the later generalization of the Mohr–Coulomb case to include dilation effects (Tremblay and Mysak, 1997). All of the rheologies discussed so far (and indeed all of those currently in use in large-scale models) assume that the ice cover is isotropic (i.e. material properties do not depend on direction). However, deformation features such as leads and ridges typically do have a preferred orientation, and so recent work by Coon *et al.* (1998) and Hibler and Schulson (2000) has focussed on the development of anisotropic rheologies that account for their effects.

9.1.2 Thermodynamics

Thermodynamic growth and melt involves the energy balance at the upper surface and underside of the ice cover, along with internal heat conduction and storage. Ice growth or melt at the ice underside results from the difference between heat conducted away from the boundary into the ice and the heat flux supplied from the ocean. At the upper surface, ice can form by submergence when the snow burden is sufficiently large; however, this surface more typically determines the heat lost from the ice in the winter (in which case the

insulating effect of snow plays an important role) and the heat gained in summer (which directly causes melt when the surface reaches the melting temperature).

Because of the vast difference between typical horizontal and vertical length-scales, sea-ice thermodynamics is generally regarded as a one-dimensional (vertical) problem. Maykut and Untersteiner (1971) provided the first comprehensive numerical model of one-dimensional sea-ice thermodynamics, and, although their numerical method was somewhat unwieldy, their model set the stage for those that followed. In particular, the simplifications introduced by Semtner (1976) are still widely used today. One-dimensional models, expanded to include multiple ice types and sophisticated parameterizations of surface processes, have been employed by Björk (1997), Ebert and Curry (1993) and Schramm *et al*. (1997) in a variety of processes using periodic, climatological forcing. Flato and Brown (1996) employed a one-dimensional thermodynamic model to study inter-annual variability in land-fast ice thickness, while Bitz and Lipscomb (1999) developed a model with a refined representation of internal heat storage (in brine pockets). Several studies have shown that assuming a linear temperature profile through the ice (i.e. not resolving the internal temperature) leads to a distortion of the seasonal cycle; however, they also show that rather few vertical layers are required to resolve the temperature profile adequately. What has become clear from work like that of Shine and Henderson-Sellers (1985) is the importance of properly representing the evolution of surface albedo during the melt season – a process still represented rather crudely in most models.

There is a large body of literature on sea-ice thermodynamics that cannot be covered adequately here; however, a recent review of thermodynamic models, their results and sensitivity analysis is available in Steele and Flato (2000).

9.1.3 Conservation equations

Sea ice moves over the surface of the ocean as a compressible material with sources/sinks of volume provided by thermodynamic evolution, and sources/sinks of area provided by divergence or convergence in the motion field. The minimum requirement is therefore a conservation equation for volume (usually in terms of mean ice thickness, h) and one for area (usually in terms of concentration, A), i.e.

$$\frac{\partial h}{\partial t} = -\nabla \cdot (\mathbf{u}h) + S_h, \tag{9.2}$$

$$\frac{\partial A}{\partial t} = -\nabla \cdot (\mathbf{u}A) + S_A, \tag{9.3}$$

where S_h and S_A are thermodynamic source terms for mean thickness and concentration, respectively. In equation (9.3) one must also enforce the constraint $A \leq 1$ (or include an additional term to guarantee this, e.g. Gray and Morland (1994)) to represent crudely the thickness buildup by ridging during convergent deformation. This is the 'two-category' representation of sea ice that was used in the model of Hibler (1979) and many others (in the literature this is often referred to as a 'two-level' model). In this case the ice strength

must be parameterized in terms of h and A only, and an approach introduced by Hibler (1979) remains the most widely used, namely

$$p = p^*h \exp[-C(1 - A)], \qquad (9.4)$$

where p^* and C are parameters often taken to be 27.5 kN/m^2 and 20, respectively.

The two-category approach ignores several important features of sea ice that are important in its mass balance, such as the non-linear effect of small-scale variations in ice thickness on thermodynamic growth (e.g. Maykut, 1978). Indeed, observations such as those made from submarine sonar indicate that a range of thickness, from open water through nearly level first- and multi-year ice, to ridged ice 10 m thick or more, may be encountered in a transect of only one kilometre in length. A framework for describing this thickness variability was proposed by Thorndike *et al.* (1975), making use of the so-called thickness distribution function, $\hat{g}(h)$. This function is analogous to the probability density function for ice thickness that evolves according to

$$\frac{\partial \hat{g}(h)}{\partial t} = -\nabla \cdot (\mathbf{u}\hat{g}) - \frac{\partial (F\hat{g})}{\partial h} + L + \psi, \qquad (9.5)$$

where F is the thermodynamic growth rate, L represents the lateral melt of ice and ψ is a 'redistribution function' that converts thin ice to thick, ridged ice during deformation. In such a formulation, energy losses associated with ridging can be accounted for in a more physically based parameterization of ice strength (Flato and Hibler, 1995; Rothrock, 1975) that is reasonably consistent with detailed ridging models (e.g. Hopkins, 1994; Hopkins and Hibler, 1991).

In practice, $\hat{g}(h)$ is typically discretized into a fixed number of thickness intervals, and so models of this sort are termed 'multi-category' models – an example of which appears in Hibler (1980). One of the principal uncertainties involves the ridge redistribution term that was explored in some detail by Flato and Hibler (1995). There are also some numerical difficulties that have been addressed recently by Bitz *et al.* (2001) and Lipscomb (2001). As a result, some global climate models are now implementing models based on this 'multi-category' formulation.

9.2 Mean thickness

Estimates of the mean spatial pattern of sea-ice thickness are available from many stand-alone models for both the Arctic and Antarctic. The details depend directly on the atmospheric forcing fields, dynamic and thermodynamic parameterizations, and the time period simulated. Figure 9.2 shows the mean March Arctic ice-thickness fields produced by four different models subjected to the same observationally based atmospheric forcing over the period 1986 to 1992. These results, obtained as part of the Sea Ice Model Intercomparison Project (SIMIP; Kreyscher, Harder and Lemke, 1997; Kreyscher *et al.*, 2000) illustrate the sensitivity of the simulated ice-thickness field to the representation of ice rheology. Three of the four rheologies (viscous–plastic, cavitating fluid and 'stoppage') are used in
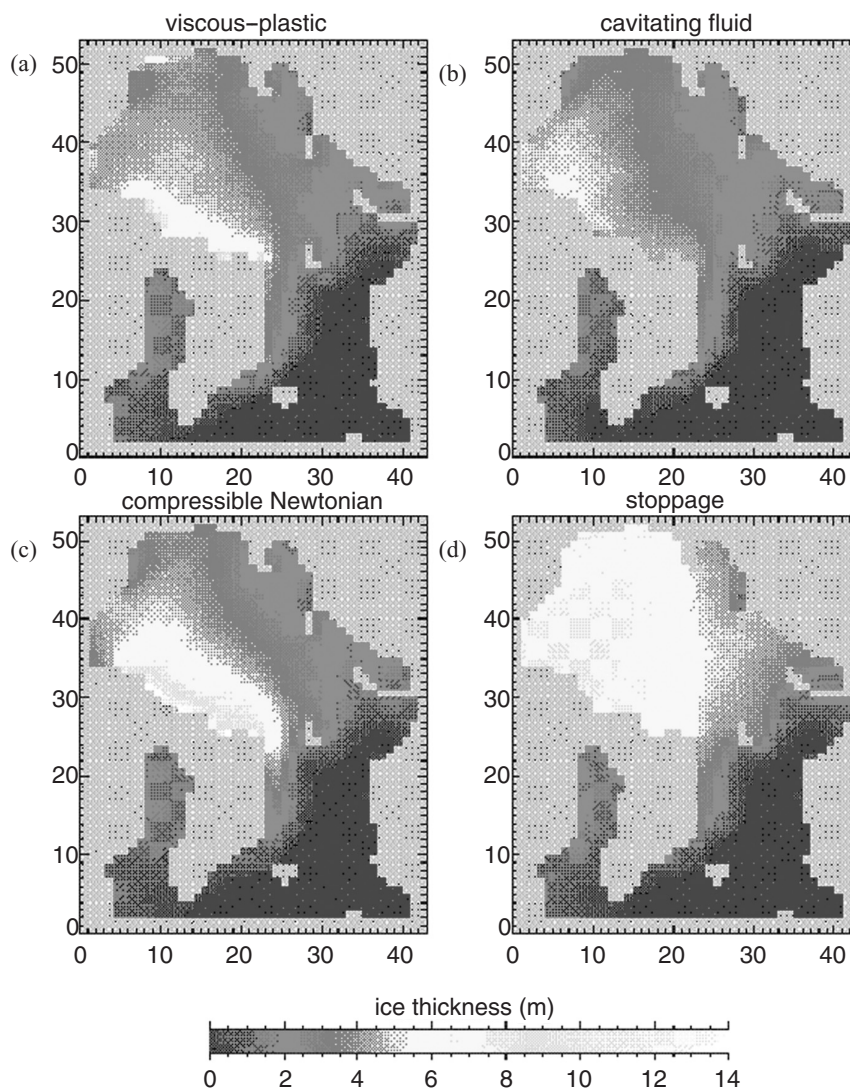
Figure 9.2. Arctic mean ice thickness for March, 1986–92, obtained using four different sea-ice models: (a) viscous–plastic; (b) cavitating fluid; (c) compressible Newtonian fluid; (d) 'stoppage' scheme, in which internal ice stress is zero when the ice thickness is less than 3 m and the ice is motionless when its thickness exceeds 3 m. See Kreyscher *et al*. (1997, 2000) for further details.

contemporary global climate models. Although the differences are substantial, all of the models exhibit a pattern of thicker ice in the North American portion of the basin, thinning toward Eurasia, especially western Eurasia, in qualitative accord with submarine observations. Kreyscher *et al*. (2000) performed a number of comparisons to available observations (thickness, velocity, etc.) and found that the viscous–plastic model performs best, followed

by the cavitating fluid model. However, it should also be noted that ice thickness, and other sea-ice quantities, are sensitive to a variety of rather poorly known parameters, allowing some opportunity for optimization ('tuning'). Such sensitivity will be discussed further in section 9.2.3.

Global climate models that include prognostic sea-ice calculations suffer not only from errors and approximations in the sea-ice component, but also from errors in the forcing provided by their atmospheric and ocean components. Many of the global climate models used to date have ignored ice motion and have treated only sea-ice thermodynamics. The Coupled Model Intercomparison Project (CMIP) affords the opportunity to compare the sea-ice simulations with several current climate models (Meehl *et al.*, 1997). Figures 9.3 and 9.4 show composite results from a subset of the CMIP model sea-ice simulations. Figures 9.3(a) and 9.4(a) display winter-time ice-cover results. The lightest shading indicates the region where less than half of the models have ice; the darkest shading indicates where more than 90% of the models have ice. In both hemispheres the 50% contour (the median ice boundary) agrees reasonably well with the observed ice edge (e.g. Gloersen *et al.*, 1992), although it should be noted that two models whose output indicated no ice in the southern hemisphere were not included. The difference between the 10% and 90% contours gives an indication of the range of modelled ice coverage. Figures 9.3(b) and 9.4(b) display the winter-time mean ice thickness averaged over twelve models in the case of the northern hemisphere and ten models in the case of the southern hemisphere. Figures 9.3(c) and 9.4(c) show the inter-model standard deviation as a measure of the range of thicknesses produced by these climate models. The northern hemisphere mean thickness is somewhat less than that inferred from observations, with maximum values of just over 2.5 m. In addition, the spatial pattern does not exhibit the pronounced increase toward North America and Greenland that is seen in Figure 9.2. This may be largely a consequence of the fact that only seven of the CMIP models include any representation of ice motion, and only four of these include a prognostic solution of the sea-ice momentum equation (the remaining three use a variant of the 'stoppage' scheme mentioned above). In addition, recent work by Bitz, Fyfe and Flato (2002) illustrates the important role of errors in GCM wind fields in simulated ice-thickness patterns for models that include ice dynamics.

9.2.1 Spatial and temporal variability

Sea ice is predominantly a 'driven' system. Although its dynamics include a non-linear rheology, with important consequences (see Chapter 7), the resulting mass balance components are largely deterministic given prescribed atmospheric and oceanic forcing. Therefore, sea-ice variability is primarily a consequence of the relatively high frequency variability imparted by the atmosphere and the relatively lower frequency variability imparted by the ocean. Of these, atmospherically driven variability has been much better studied.

Spatial variations in ice motion result in deformation which, over timescales up to a few days, dominate the local opening and closing so important to ice growth. This high
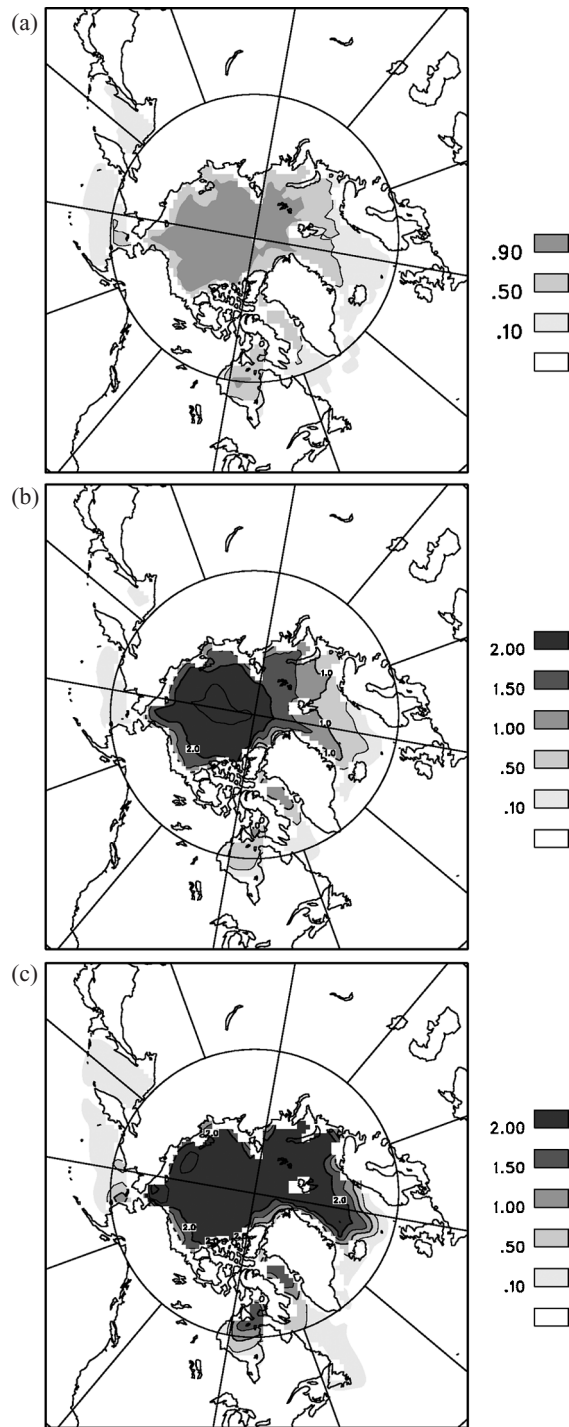
Figure 9.3. Arctic winter-time (December–February) sea-ice results from the coupled model inter-comparison project (CMIP). (a) 10, 50 and 90 percentile ice-cover boundaries obtained from 14 of the participating models. (b) Model ensemble mean ice thickness and (c) inter-model thickness standard deviation obtained from 12 of the participating models.
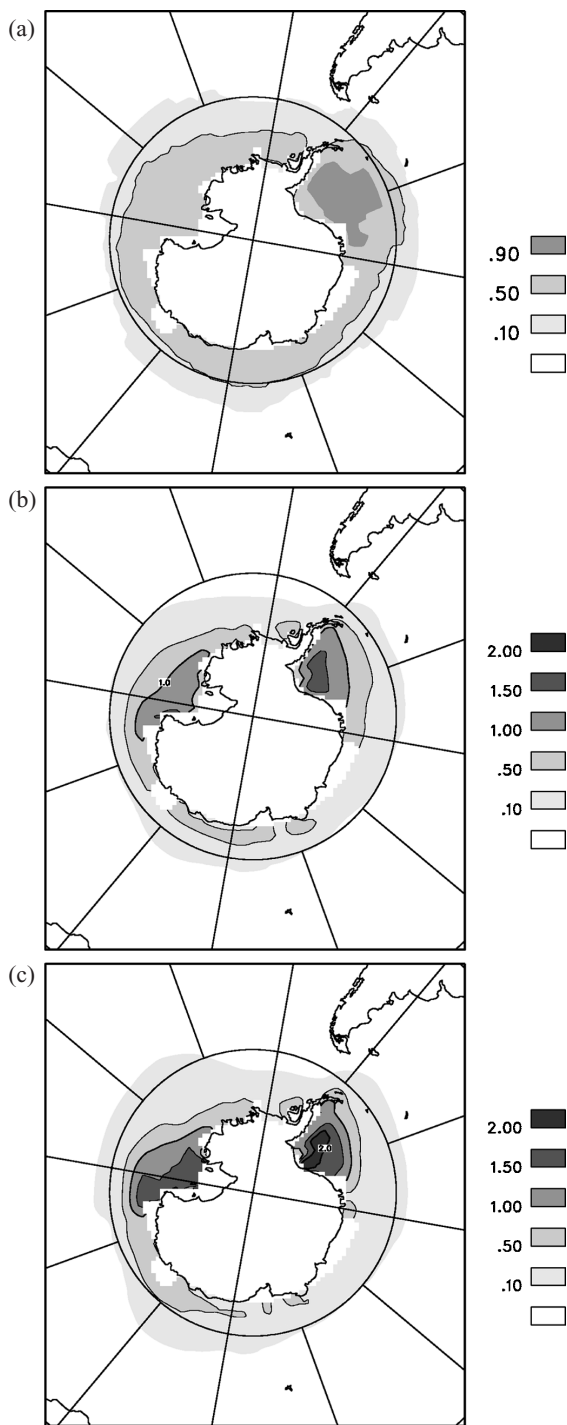
Figure 9.4. Antarctic winter-time (June–August) sea-ice results from the coupled model intercomparison project (CMIP). (a) 10, 50 and 90 percentile ice-cover boundaries obtained from 12 of the participating models. (b) Model ensemble mean ice thickness and (c) inter-model thickness standard deviation obtained from ten of the participating models.

frequency motion includes synoptic forcing from the atmosphere and, in some locations, important contributions from tidal and inertial oscillations (e.g. Geiger *et al.*, 1998; Heil and Hibler, 2002). At longer timescales, ice transport variations lead to large-scale variability in ice thickness and net freezing rate. The forcing in this case is related to large-scale modes of variability in the atmosphere (such as the North Atlantic oscillation, NAO, and the Arctic Oscillation, AO), and, for the Arctic at least, this kind of ice-motion variability has received considerable attention recently (e.g. Maslowski *et al.*, 2000; Polyakov, Proshutinsky and Johnson, 1999; Proshutinsky and Johnson, 1997; Proshutinsky, Polyakov and Johnson, 1999; Zhang, Rothrock and Steele, 2000). The picture that emerges is one of variations between a large Beaufort gyre (much as in Figure 9.1) that spans most of the western Arctic, and a much smaller gyre confined to the Beaufort Sea proper.

Arctic ice-thickness variability, forced primarily by variations in wind-driven deformation and transport, appears to have a characteristic pattern, illustrated in Figure 9.5 (from Hilmer and Lemke (2000)). This figure shows the inter-annual standard deviation of ice thickness
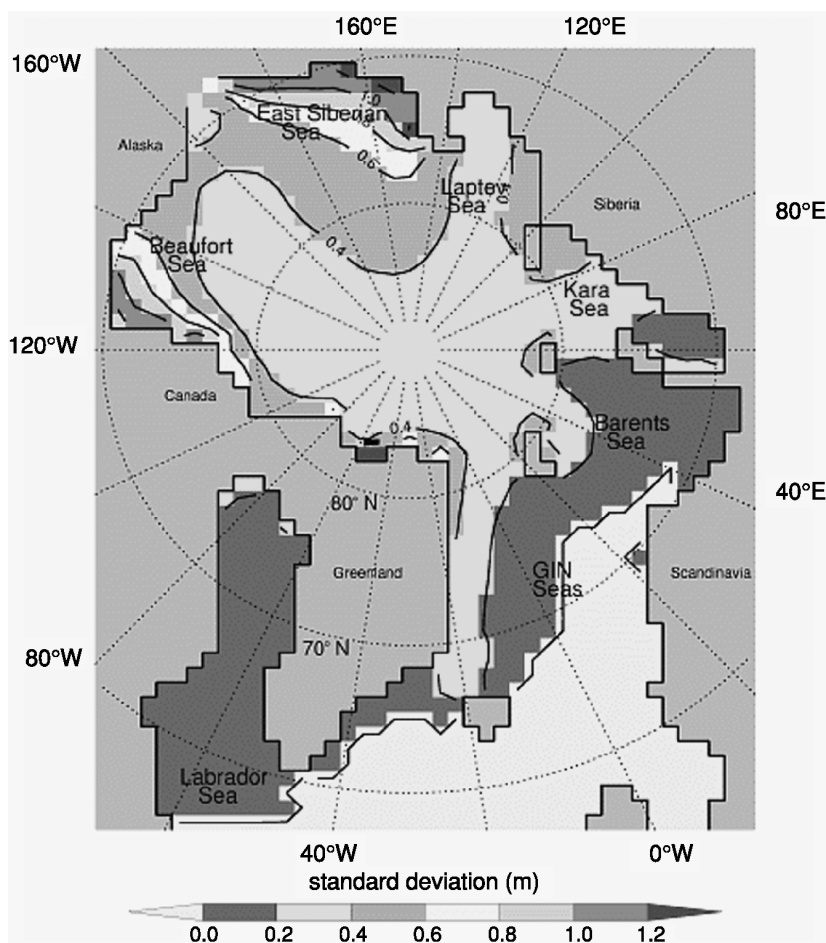

Figure 9.5. Inter-annual standard deviation of Arctic mean ice thickness (Hilmer and Lemke, 2000).

obtained from a 40-year ice model simulation. A similar result, using a different model, was obtained by Flato (1995). The variability is largest in the Beaufort and East Siberian Seas, and appears to result primarily from simultaneous thick anomalies in one region and corresponding thin anomalies in the other. Zhang *et al.* (2000) term this the 'east–west Arctic anomaly pattern' (EWAAP).

Temporal variability of Arctic ice volume cannot, so far, be estimated from observations, but it has been examined in various model studies. Arctic basin-scale studies, using observationally based forcing fields spanning several decades, have been performed (e.g. Chapman *et al.*, 1994; Flato, 1995; Häkkinen, 1993; Hilmer and Lemke, 2000; Walsh, Hibler and Ross, 1985), as have century or longer simulations with one-dimensional models (e.g. Bitz *et al.*, 1996; Häkkinen and Mellor, 1990; Holland and Curry, 1999). In either case, the simulated ice volume varies predominantly on inter-decadal and longer timescales. Some studies have concluded that variations in thermodynamic forcing (pole-ward heat transport by the atmosphere) dominate, while others have pointed toward variability in wind-driven deformation. Thermodynamic forcing is amplified by positive albedo feedbacks, which are rather sensitive to details of the model parameterizations (Battisti, Bitz and Moritz, 1997). On the other hand, ridging processes, creating thick ice that survives for many years, may act to damp out forced variability (Holland and Curry, 1999). Figure 9.6 illustrates this effect with the temporal auto-correlation function of simulated Arctic ice volume from a model that included an explicit representation of the thickness distribution function (Flato, 1995). One sees that the correlation timescale for thin ice (<1 m) is approximately two months, for medium ice (2 to 5 m) the timescale is about 20 months, whereas for the total ice volume, the timescale is roughly seven years. The reason is that thick, ridged ice (which accounts for nearly half of the simulated ice volume) is able to survive many summer melt seasons before ultimately being exported from the Arctic.
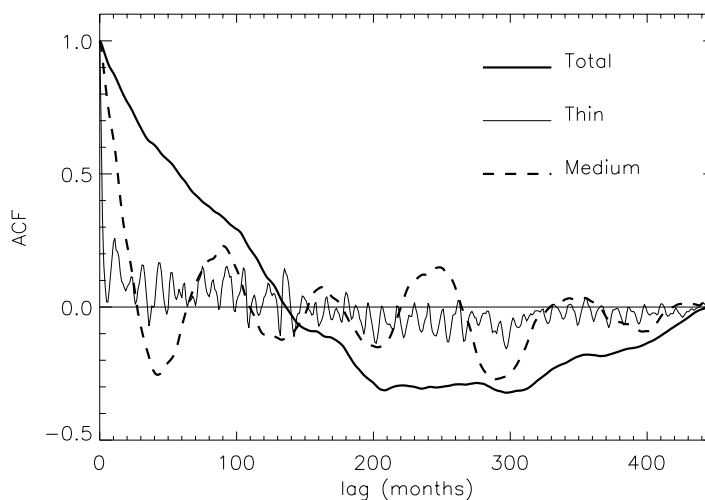

Figure 9.6. Auto-correlation functions (ACF) of total, medium (2 to 5 m) and thin (<1 m) ice Arctic sea-ice volume anomaly time series (Flato, 1995).

Knowledge of temporal and spatial variability in ice thickness is important in interpreting rather sparse observations from submarines. Wadhams (1990) compared submarine observations from 1976 and 1987 which showed a 15% decrease in ice thickness in a region north of Greenland. From Figure 9.5 one sees that a model-based estimate of the inter-annual standard deviation near the north Greenland coast is in excess of 0.4 m (where the modelled and observed mean thickness is roughly 6 m). So, sampling variability provides one 'explanation' for the observed decrease and is, in any case, the null hypothesis to be rejected. In a more recent comparison of submarine observations over much of the central Arctic, Rothrock, Yu and Maykut (1999) found a roughly 40% decrease in thickness between the 1960s and 1990s averaged over 29 locations where a comparison could be made. In a recent study (Holloway and Sou, 2002), the ice thickness obtained from a model run over the same period was sampled in the same way as the observations. The thickness change at the sample locations agreed well with the observed change, but, interestingly, the overall volume change was only about 12% (broadly commensurate with the observed 3% per decade decline in Arctic ice extent). Figure 9.7 displays the modelled ice-thickness
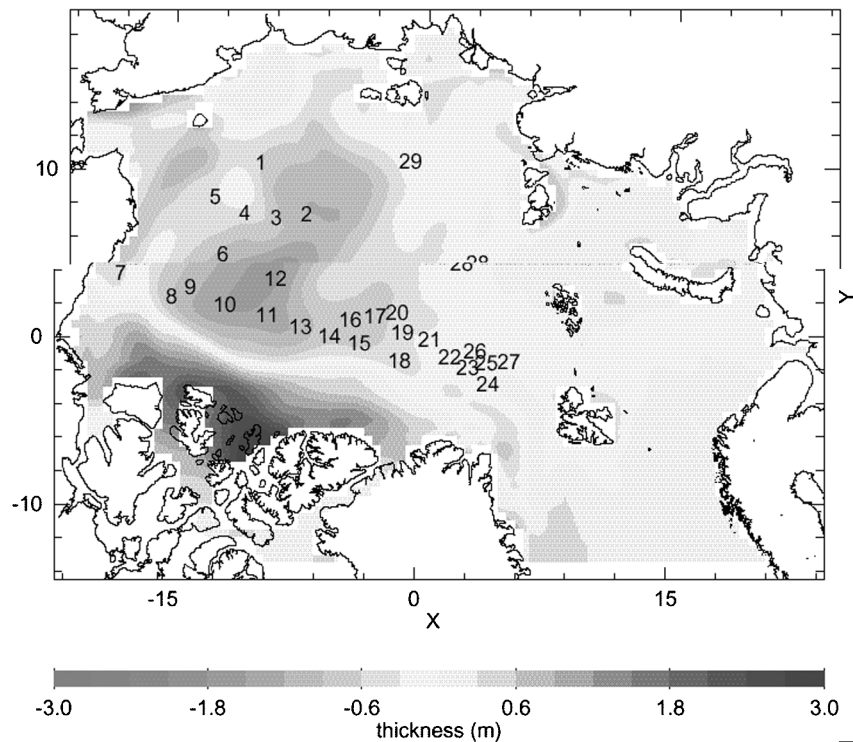

Figure 9.7. Change in modelled ice thickness obtained as the average of years 1993, 1996 and 1997, minus 1958, 1960, 1962, 1970 and 1976. The numbers indicate the locations of the submarine-derived differences used by Rothrock *et al*. (1999). (Figure provided by G. Holloway (Holloway and Sou, 2002).)

change over the period compared by Rothrock *et al*. (1999); it shows that the spatial distribution of thickness changed substantially (in a manner consistent with Figure 9.5), and that the submarine observations coincidentally sampled only the region that experienced thinning.

9.2.2 Ice export

In both the Arctic and the Antarctic, net ice growth is, over the long term, balanced by transport. In the Antarctic ice is generally transported northward away from the continent, and thus the export is not localized (e.g. Stössel, Lemke and Owens, 1990). Antarctic model studies have primarily focussed on ice export in the Weddell Sea (e.g. Harder and Fischer, 1999). In the Arctic most export passes through the Fram Strait, and several model studies have focussed on Fram Strait export and its variability. An example, based on Hilmer *et al*. (1998), is provided in Figure 9.8 and shows a time series of simulated annual mean ice export anomalies from 1958 to 1997. Studies like this have shown that ice export variability is primarily driven by local wind forcing which, by virtue of proximity to the Icelandic low, is connected to the North Atlantic oscillation. Indeed, Kwok and Rothrock (1999) demonstrate a significant correlation between the NAO index and observationally based estimates of Fram Strait ice area flux. However, a recent model study by Hilmer and Jung (2000) indicates that the correlation between the NAO and Fram Strait ice export was considerably weaker in the past, owing to rather subtle shifts in NAO-related wind patterns.

Because the export of sea ice from the Arctic is such an important source of fresh water to the North Atlantic, large anomalies in ice export may have profound impacts on ocean stratification and convection. A particular episode of anomalously large export, associated with the 'great salinity anomaly' of the late 1960s, has received particular attention (e.g. Dickson *et al*., 1988). Model studies such as those of Häkkinen (1993) and Hilmer *et al*. (1998) have illustrated the role of local and regional atmospheric forcing in events such as this, and in low frequency outflow variability in general.
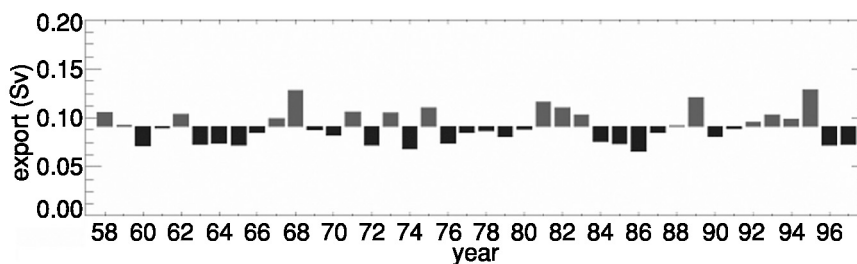

Figure 9.8. Simulated annual mean Fram Strait ice export anomalies. Export is measured in 'Sverdrups' (sv), defined as 10^6 m^3/s. (From Hilmer *et al*. (1998).)

9.2.3 Sensitivity to model parameterizations

The modelled sea-ice mass balance components depend directly on assumptions, approximations and parameterizations of unresolved physical processes. Because many of the relevant parameters are poorly constrained by observations (and some, like geophysical-scale ice strength, are virtually impossible to measure directly), the uncertainties imbued on model variables have typically been assessed by conducting sensitivity studies (e.g. Holland, Mysak and Manak, 1993). In the case of ice or ice–ocean models, the results are of course also sensitive to errors in the prescribed atmospheric (and oceanic) forcing.

Perhaps the least constrained parameterizations involve representation of internal ice stresses. The resistance to deformation afforded by large-scale ice dynamics is a significant term in the sea-ice momentum balance (e.g. Steele *et al*., 1997), and thus plays an important role in simulated ice motion (e.g. Flato and Hibler, 1992) and the resulting thickness buildup pattern illustrated in Figure 9.2. Resistance of sea ice to deformation is characterized by a 'yield curve' representing the locus of stress states separating nearly rigid behaviour from plastic flow (see Chapter 7 for details). The yield curve must be specified in a model, and the dependence of simulated thickness and motion statistics on yield curve shape has been investigated by Ip *et al*. (1991) and Kreyscher *et al*. (1997, 2000). The results so far have indicated that a plastic rheology with a yield curve similar to the ellipse proposed by Hibler (1979) compares most favourably with a range of observations. A closely related issue is the parameterization of ice strength. For the widely used 'two-category' representation of ice thickness, a parameterization based on mean thickness and concentration is used (equation (9.4)); in 'multi-category' models, a parameterization based on energy losses during ridging is used (Rothrock, 1975). The parameter values are typically chosen by comparison to buoy drift observations (e.g. Hibler and Walsh, 1982), but the two parameterizations produce significantly different results when compared directly in the same model (Flato, 1996). In multi-category models, the strength parameterization is closely coupled to the representation of ice ridging, further complicating efforts to optimize parameter values (Flato and Hibler, 1995).

Thermodynamic parameterizations also have a significant impact on modelled sea-ice mass balance components, particularly as they directly affect ice growth and melt. Various authors have performed sensitivity studies related to parameterizations involving surface albedo (e.g. Curry, Schramm and Ebert, 1995), thermal conductivity (e.g. Fichefet, Tartinville and Goosse, 2000), heat capacity (Bitz and Lipscomb, 1999), snow-cover effects (e.g. Fichefet and Morales Maqueda, 1999), the inclusion of multiple thickness categories (e.g. Schramm *et al*., 1997) and the potential role of two-dimensional heat conduction effects in ridged ice (Schramm, Flato and Curry, 2000). Representation of lead thermodynamics, frazil ice formation,[1] multi-year ice metamorphosis and other potentially important processes remain rather poorly explored. A detailed review of all such studies is beyond the scope of this chapter; however, results from a recent study using

---

[1] Frazil ice forms in turbulent supercooled water and consists of small platelets roughly 1 mm in diameter. These platelets ultimately clump together and consolidate as cooling continues.

Table 9.1. *Importance of sea-ice processes in each hemisphere.*

Process	Northern hemisphere	Southern hemisphere
Internal heat storage	unimportant	unimportant
Brine pocket storage	important	unimportant
Penetrating short-wave radiation	important	unimportant
Sub-grid-scale variability in heat conduction	important	important
Snow cover	unimportant	important
Snow ice formation (by submergence)	unimportant	important
Lead formation	important	important
Ice motion/deformation	important	important
Resistance to shear	intermediate	unimportant

Adapted from Fichefet and Morales Maqueda (1997).

a global ice–upper ocean model (Fichefet and Morales Maqueda, 1997), summarized in Table 9.1, are instructive. Although by no means definitive, the use of a global model allows the relative importance of various processes (judged in a qualitative manner) to be compared for the northern and southern hemispheres.

Although only a subjective assessment from one model, the results in Table 9.1 indicate that sub-grid-scale variability in heat exchange, due to variations in ice thickness and snow cover, play an important role in both hemispheres, as do processes related to ice motion, deformation and lead formation. Because of the larger snow-fall rates and thinner ice, snow processes play a bigger role in the southern hemisphere ice cover. On the other hand, thicker, longer-lived ice in the northern hemisphere is more strongly affected by processes involving penetration of short-wave radiation into the ice, and the latent heat exchange between brine pockets and the surrounding ice.

9.3 Modelling future changes in sea-ice mass balance

Climate model simulations and recent observations agree that surface air temperature increases due to enhanced greenhouse gas forcing are largest at high latitudes. This pole-ward amplification of warming is apparent in projections of future climate change (e.g. Kattenberg *et al*., 1996), and is in large part a consequence of sea-ice-related feedbacks (e.g. Rind *et al*., 1995). Corresponding reductions in sea-ice thickness and extent are therefore anticipated. As an example, Figure 9.9 compares northern and southern hemisphere annual mean sea-ice extent simulated by two global climate models over the period 1900 to 2100 using the same historical and 'business as usual' future scenario for greenhouse gas and aerosol forcing. The curve labelled CGCM2 refers to the second-generation model of the Canadian Centre for Climate Modelling and Analysis (Flato and Boer, 2001); the curve
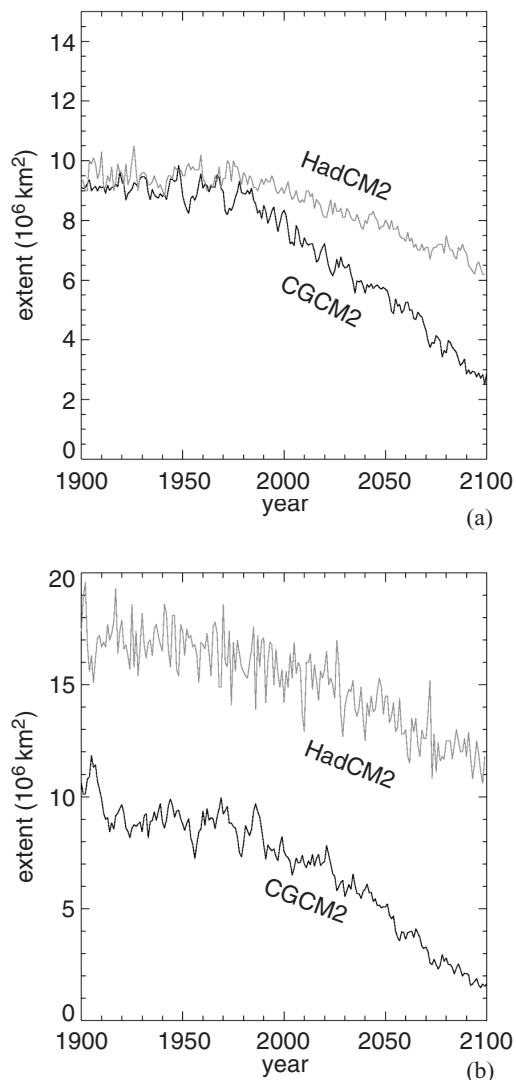
Figure 9.9. Simulated annual mean sea-ice extent for the northern (a) and southern (b) hemispheres. Results from CGCM2 and HadCM2 are shown.

labelled HadCM2 refers to the second-generation model of the Hadley Centre for Climate Prediction and Research (Johns *et al.*, 1997). Both models include a representation of sea-ice motion (cavitating fluid in the case of CGCM2 and 'stoppage' in the case of HadCM2). Both models under-estimate the historical northern hemisphere sea-ice extent (observed to be roughly 13×10^6 km^2), but are split on southern hemisphere extent (observed to be roughly 14×10^6 km^2). The results shown in Figures 9.3 and 9.4 indicate that errors of this magnitude are not uncommon in current-generation climate models, owing largely to the
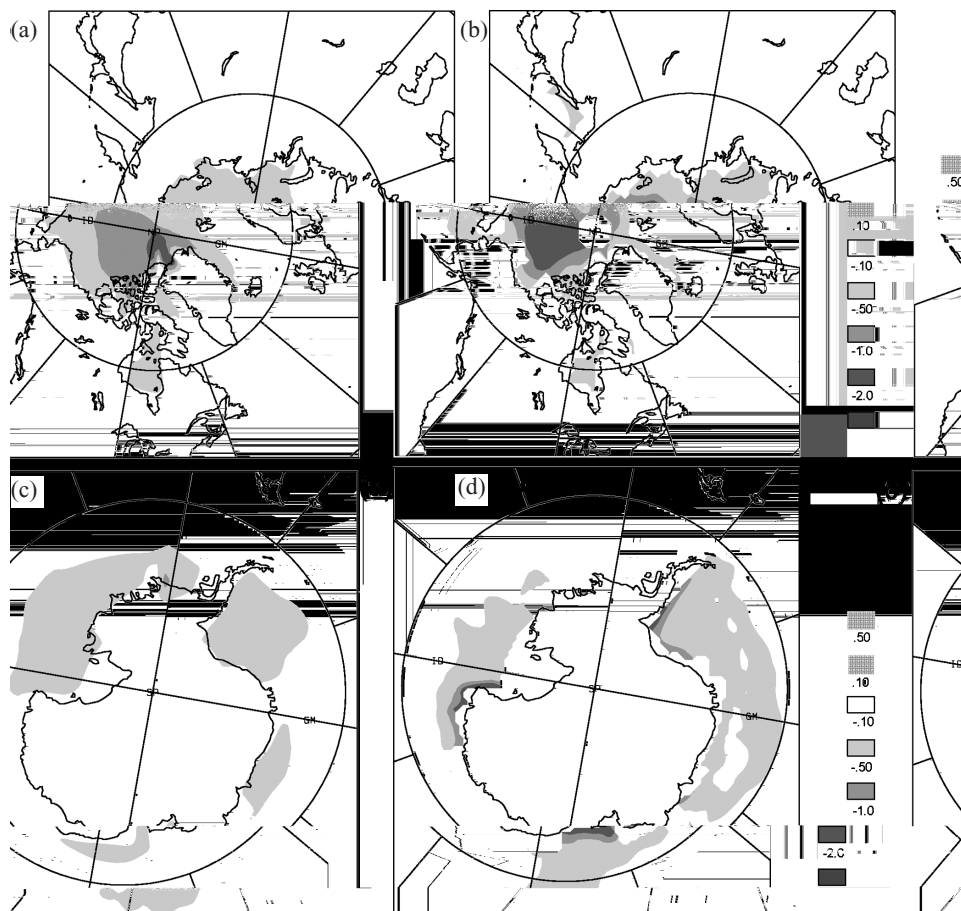
Figure 9.10. Simulated change in winter-time sea-ice thickness in the northern and southern hemi-spheres. (a), (c) Results from CGCM2. (b), (d) Results from HadCM3.

sensitivity of ice extent to the subtle balance of heat in the atmosphere and ocean near the ice edge. Nevertheless, both models are in general agreement with the observed northern hemisphere decline of 3% per decade since 1978 (e.g. Cavalieri *et al.*, 1997), although CGCM2 projects a much more rapid future decline than does HadCM2. Vinnikov *et al.* (1999) provide more detailed analysis of results like these for the northern hemisphere. In the southern hemisphere, the two models agree more closely with regard to the future trend if one removes their respective historical biasses.

Projected changes in ice thickness can also be obtained from global models. Figure 9.10 displays the change in thickness between 1971 and 1990 and 2041 and 2060 for winter-time in both hemispheres (December to February in the northern hemisphere and June to July in the southern hemisphere). Results on the left hand side of the figure are from CGCM2, described above, while those on the right are from a more recent version of the Hadley

Centre model, HadCM3 (Gordon *et al.*, 2000). The two models agree reasonably well in terms of both the magnitude and spatial pattern of the thickness change, with values greater than 0.5 m over the central Arctic and less than 0.5 m over almost all of the Antarctic ice pack.

The model results discussed above project a continuing decline in ice thickness and extent as the climate warms – persistent negative mass balance. Of course, these are only two of many available climate models, and, while they agree qualitatively, the magnitude of the projected decline and its spatial pattern differ. The results shown earlier in Figures 9.3 and 9.4 indicate substantial variation in coupled climate model simulations of contemporary sea-ice extent and thickness, and this inter-model spread reflects the cumulative effect of differences in a whole range of model details (atmosphere, ocean and sea ice). These differences also affect the response of modelled sea ice to climate forcing. That is, a model projection of future climate change depends in part on the response of the sea-ice component to climatic perturbations (as distinct from the response of the mean state to model parameters).

Various model studies have attempted to estimate the potential effect of sea-ice parameterizations on climate sensitivity (e.g. Arbetter, Curry and Maslanik, 1999; Flato, 1998; Hibler, 1984; Holland, 1998; Pollard and Thompson, 1994). Although the experiments differ substantially in terms of model domain, applied perturbation and variable(s) analysed, the general impression is that including dynamics tends to decrease sea-ice sensitivity to perturbations, whereas including a representation of the thickness distribution increases or decreases the sensitivity depending on the details of the experiment performed and the particular diagnostic quantity used to measure the model's response. In any case, it remains difficult to anticipate the impact of a change in sea-ice parameterization once all the feedbacks of a coupled ocean–ice–atmosphere model are included. Results of model inter-comparison studies will continue to be valuable in this regard.

9.4 Summary and conclusions

Numerical models encapsulate much of what is known about the physics of sea ice, and thereby provide a means of investigating the role of various processes. In addition, when driven by observationally based atmospheric and oceanic forcing, such models provide estimates of quantities not easily observable. Finally, when used in the context of global climate simulations, such models provide projections of future changes in sea-ice conditions and behaviour.

Stand-alone models are able to produce credible estimates of the spatial pattern and temporal evolution of sea-ice thickness, its transport and deformation, and net growth and melt. In many cases, these mass balance components are poorly observed, and so model results may aid in the interpretation of the sparse observations that are available. The potential for a more formal combination of observations and models, via data assimilation techniques, has not so far been realized, although some initial attempts have been made (e.g. Meier, Maslanik and Fowler, 2000; Thomas *et al.*, 1996). Sea-ice mass balance estimates using data assimilation methods are likely to become more widespread in the future. Data assimilation

could also be used to improve estimates of various model parameters, particularly those related to geophysical-scale mechanical properties which are otherwise virtually impossible to measure directly.

Global climate models necessarily include a sea-ice component, although often employing parameterizations that are less sophisticated than those in 'state-of-the-art' stand-alone models. In the case of climate models, the discrepancies between modelled and observed sea-ice features, and differences from one model to another, are due not only to errors and uncertainties in the sea-ice component, but also to errors in the atmospheric, oceanic and even terrestrial components of the model. Many global modelling centres have or are introducing substantial improvements into the sea-ice component of their climate models, in particular through the use of more sophisticated treatments of sea-ice dynamics and multi-layer formulations of vertical heat conduction. The on-going atmospheric and coupled model inter-comparison projects will allow the impact of these improvements to be assessed.

Climate model projections generally indicate enhanced warming at high latitudes, with a corresponding decline in ice extent and thickness. However, the rate of decline and the strength of the various feedbacks that enhance or damp the warming response are highly uncertain. Observations aimed at testing and improving sea-ice parameterizations, and at evaluating modelled trends and variability, will continue to be important in refining projections of future changes in the sea-ice mass balance.

References

Arbetter, T. E., Curry, J. A. and Maslanik, J. A. 1999. Effects of rheology and ice thickness distribution in a dynamic-thermodynamic sea ice model. *J. Phys. Oceanography* **29**, 2656–70.

Battisti, D. S., Bitz, C. M. and Moritz, R. E. 1997. Do general circulation models underestimate the natural variability in the Arctic climate? *J. Climate* **10**, 1909–20.

Bitz, C. M. and Lipscomb, W. H. 1999. An energy-conserving thermodynamic model of sea ice. *J. Geophys. Res*. **104**, 15 669–77.

Bitz, C. M., Fyfe, J. C. and Flato, G. M. 2002. Sea ice response to wind forcing from AMIP models. *J. Climate* **15**, 522–36.

Bitz, C. M., Battisti, D. S., Moritz, R. E. and Besley, J. A. 1996. Low-frequency variability in the Arctic atmosphere, sea ice, and upper-ocean climate system. *J. Climate* **9**, 394–408.

Bitz, C. M., Holland, M. M., Weaver, A. J. and Eby, M. 2001. Simulating the ice-thickness distribution in a coupled climate model. *J. Geophys. Res.* **106**, 2441–64.

Björk, G. 1997. The relation between ice deformation, oceanic heat flux, and the ice thickness distribution in the Arctic Ocean. *J. Geophys. Res*. **102**, 18 681–98.

Campbell, W. J. 1965. The wind-driven circulation of ice and water in a polar ocean. *J. Geophys. Res*. **70**, 3279–301.

Cavalieri, D. J., Gloersen, P., Parkinson, C. L., Comiso, J. C. and Zwally, H. J. 1997. Observed hemispheric asymmetry in global sea ice changes. *Science* **278**, 1104–6.

Chapman, W. L., Welch, W. J., Bowman, K. P., Sacks, J. and Walsh, J. E. 1994. Arctic sea ice variability: model sensitivities and a multi-decadal simulation. *J. Geophys. Res*. **99**, 919–35.

Coon, M. D., Knoke, G. S., Echert, D. C. and Pritchard, R. S. 1998. The architecture of an anisotropic elastic-plastic sea ice mechanics constitutive law. *J. Geophys. Res.* **103**, 21 915–25.

Curry, J. A., Schramm, J. L. and Ebert, E. E. 1995. Sea ice-albedo climate feedback mechanism. *J. Climate* **8**, 240–7.

Dickson, R. R., Meinke, J., Malmberg, S. A. and Lee, A. J. 1988. The 'great salinity anomaly' in the northern North Atlantic 1968–1982. *Prog. Oceanography* **20**, 103–51.

Ebert, E. E. and Curry, A. J. 1993. An intermediate one-dimensional thermodynamic sea ice model for investigating ice-atmosphere interactions. *J. Geophys. Res*. **98**, 10 085–110.

Fichefet, T. and Morales Maqueda, M. A. 1997. Sensitivity of a global sea ice model to the treatment of ice thermodynamics and dynamics. *J. Geophys. Res*. **102**, 12 609–46.
   1999. Modelling the influence of snow accumulation and snow-ice formation on the seasonal cycle of the Antarctic sea-ice cover. *Climate Dyn.* **15**, 251–68.

Fichefet, T., Goosse, H. and Morales Maqueda, M. A. 1998. On the large-scale modelling of sea ice and sea ice – ocean interactions. In Chassignet, E. P. and Verron, J., eds., *Ocean Modeling and Parameterization*. Dordrecht, Kluwer, pp. 399–422.

Fichefet, T., Tartinville, B. and Goosse, H. 2000. Sensitivity of the Antarctic sea ice to thermal conductivity. *Geophys. Res. Lett*. **27**, 401–4.

Flato, G. M. 1995. Spatial and temporal variability of Arctic ice thickness. *Ann. Glaciol*. **21**, 323–9.
   1996. Parameterizing the strength of Arctic sea ice. *Proceedings of the ACSYS Conference on the Dynamics of the Arctic Climate System*, Göteborg, Sweden. November 7–10, 1994. World Climate Research Programme, WMO/TD no. 760, pp. 278–82.
   1998. The sensitivity of models in the SIMIP hierarchy to thermodynamic perturbations. *Proc of the ACSYS Conference on Polar Processes and Global Climate*, Orcas Island, USA, November 3–6, 1997. World Climate Research Programme, WMO/TD no. 908, pp. 51–3.

Flato, B. M. and Boer, G. J. 2001. Warming asymmetry in climate change simulations. *Geophys. Res. Lett*. **28**, 195–8.

Flato, G. M. and Brown, R. D. 1996. Variability and climate sensitivity of landfast Arctic sea ice. *J. Geophys. Res*. **101**, 25 767–77.

Flato, G. M. and Hibler, W. D. III. 1992. Modeling pack ice as a cavitating fluid. *J. Phys. Oceanography* **22**, 626–51.
   1995. Ridging and strength in modeling the thickness distribution of Arctic sea ice. *J. Geophys. Res*. **100**, 18 611–26.

Geiger, C. A., Hibler, W. D. III and Ackley, S. F. 1998. Large-scale sea ice drift and deformation: comparison between models and observations in the western Weddell Sea during 1992. *J. Geophys. Res*. **103**, 21 893–913.

Gloersen, P., Campell, W. J., Cavalieri, D. J., Comiso, J. C., Parkinson, C. L. and Zwally, H. J. 1992. Arctic and Antarctic sea ice, 1978–1987: satellite passive microwave observations and analysis. NASA SP-511, 290 pp.

Gordon, C. *et al.* 2000. The simulation of SST, sea ice extents and ocean heat transports in a version of the Hadley Centre coupled model without flux adjustments. *Climate Dyn.* **16**, 147–68.

Gray, J. M. N. T. and Morland, L. W. 1994. A two-dimensional model for the dynamics of sea ice. *Phil. Trans. Roy. Soc. London A* **347**, 219–90.

Häkkinen, S. 1993. An Arctic source for the great salinity anomaly: a simulation of the Arctic ice-ocean system for 1955–1975. *J. Geophys. Res*. **98**, 16 397–410.

Häkkinen, S, and Mellor, G. L. 1990. One hundred years of Arctic ice cover variations as simulated by a one-dimensional, ice-ocean model. *J. Geophys. Res*. **95**, 15 959–69.

Harder, M. and Fischer, H. 1999. Sea ice dynamics in the Weddell Sea simulated with an optimized model. *J. Geophys. Res*. **104**, 11 151–62.

Heil, P. and Hibler, W. D. III. 2002. Modeling the high-frequency component of Arctic sea-ice drift and deformation, *J. Phys. Oceanography* **32**, 3039–57.

Hibler, W. D. III. 1974. Differential sea ice drift. II: comparison of mesoscale strain measurements to linear drift theory predictions. *J. Glaciol*. **13**, 457–71.

   1979. A dynamic thermodynamic sea ice model. *J. Phys. Oceanography* **9**, 817–46.

   1980. Modeling a variable thickness sea ice cover. *Month Weather Rev*. **108**, 1943–73.

   1984. The role of sea ice dynamics in modeling CO_2 increases. *Climate Processes and Climate Sensitivity*. Geophysical Monograph 29. American Geophysical Union, pp. 238–53.

   1986. Ice dynamics. In Untersteiner, N., ed., *Geophysics of Sea Ice*. New York, Plenum Press, pp. 577–640.

Hibler, W. D. III and Flato, G. M. 1992. Sea ice models. In Trenberth, K. E., ed., *Climate System Modeling*. Cambridge University Press, pp. 413–36.

Hibler, W. D. III and Schulson, E. M. 2000. On modelling the anisotropic failure and flow of flawed sea ice. *J. Geophys. Res*. **105**, 17 105–20.

Hibler, W. D. III and Walsh, J. E. 1982. On modeling seasonal and interannual fluctuations of Arctic sea ice. *J. Phys. Oceanography* **12**, 1514–23.

Hilmer, M. and Jung, T. 2000. Evidence for a recent change in the link between the North Atlantic oscillation and Arctic sea ice export. *Geophys. Res. Lett*. **27**, 989–92.

Hilmer, M. and Lemke, P. 2000. On the decrease of Arctic sea ice volume. *Geophys. Res. Lett.* **27**, 3751–4.

Hilmer, M., Harder, M. and Lemke, P. 1998. Sea ice transport: a highly variable link between Arctic and North Atlantic. *Geophys. Res. Lett*. **25**, 3359–62.

Holland, D. M., Mysak, L. A. and Manak, D. K. 1993. Sensitivity study of a dynamic thermodynamic sea ice model. *J. Geophys. Res*. **98**, 2561–86.

Holland, M. M. 1998. The impact of the ice thickness distribution on simulated Arctic budgets and climate. *Proceeding of the ACSYS Conference on Polar Processes and Global Climate*, Orcas Island, USA, November 3–6, 1997. World Climate Research Programme, WMO/TD no. 908, pp. 93–5.

Holland, M. M. and Curry, J. A. 1999. The role of physical processes in determining the interdecadal variability of central Arctic sea ice. *J. Climate* **12**, 3319–30.

Holloway, G. and Sou, T. 2002. Is Arctic sea ice rapidly thinning? *J. Climate* **15**, 1691–1701.

Hopkins, M. A. 1994. On the ridging of intact lead ice. *J. Geophys. Res*. **99**, 16 351–60.

Hopkins, M. A. and Hibler, W. D. III. 1991. On the ridging of a thin sheet of lead ice. *Ann. Glaciol*. **15**, 81–6.

Hunke, E. C. and Dukowicz, J. K. 1997. An elastic-viscous-plastic model for sea ice dynamics. *J. Phys. Oceanography* **27**, 1849–67.

Ip, C. F., Hibler, W. D. III and Flato, G. M. 1991. On the effect of rheology on seasonal sea-ice simulations. *Ann. Glaciol*. **15**, 17–25.

Johns, T. C. *et al*. 1997. The second Hadley Centre coupled ocean-atmosphere GCM: model description, spinup and validation. *Climate Dyn.* **13**, 103–34.

Kattenberg, A. *et al.* 1996. Climate models – projections of future climate. In Houghton, J. *et al.*, eds., *Climate Change 1995. The Science of Climate Change*. Cambridge University Press, pp. 285–358.

Kreyscher, M., Harder, M. and Lemke, P. 1997. First results of the sea-ice model intercomparison project (SIMIP). *Ann. Glaciol.* **25**, 8–11.

Kreyscher, M., Harder, M., Lemke, P. and Flato, G. M. 2000. Results of the sea ice model intercomparison project: evaluatoin of sea-ice rheology schemes for use in climate simulations. *J. Geophys. Res*. **105** (C5), 11 299–320.

Kwok, R. and Rothrock, D. A. 1999. Variability of Fram Strait ice flux and North Atlantic oscillation. *J. Geophys. Res*. **104**, 5177–89.

Lipscomb, W. H. 2001. Remapping the thickness distribution in sea ice models. *J. Geophys. Res*. **106**, 13 989–14 000.

Maslowski, W., Newton, B., Schlosser, P., Semtner, A. and Martinson, D. 2000. Modeling recent climate variability in the Arctic Ocean. *Geophys. Res. Lett*. **27**, 3743–6.

Maykut, G. A. 1978. Energy exchange over young sea ice in the central Arctic. *J. Geophys. Res*. **83**, 3646–58.

Maykut, G. A. and Untersteiner, N. 1971. Some results from a time-dependent thermodynamic model of sea ice. *J. Geophys. Res*. **76**, (6) 1550–75.

Meehl, G. A., Boer, G. J., Covey, C., Latif, M. and Stouffer, R. J. 1997. Intercomparison makes for a better climate model. *EOS, Trans. Am. Geophys. Union* **78**, 445–6.

Meier, W. N., Maslanik, J. A. and Fowler, C. W. 2000. Error analysis and assimilation of remotely sensed ice motion within an Arctic sea ice model. *J. Geophys. Res*. **105**, 3339–56.

Moritz, R. E. and Stern, H. L. 2001. Relationships between geostrophic winds, ice strain rates and the piecewise rigid motions of pack ice. In Dempsey, J. P. and Shen, H. H., eds., *Proceedings of the IUTAM Symposium on Scaling Laws in Ice Mechanics and Ice Dynamics*, Fairbanks, June 13–16, 2000. Dordrecht, Kluwer.

Moritz, R. E. and Ukita, J. 2000. Geometry and the deformation of pack ice, Part I: a simple kinematic model. *Ann. Glaciol.* **31**, 313–22.

Pollard, D. and Thompson, S. L. 1994. Sea-ice dynamics and CO_2 sensitivity in a global climate model. *Atmos.-Ocean* **32**, 449–63.

Polyakov, I. V., Proshutinsky, A. Y. and Johnson, M. A. 1999. Seasonal cycles in two regimes of Arctic climate. *J. Geophys. Res*. **104**, 25 761–88.

Polyakov, I. V. *et al.* 1998. Coupled sea ice-ocean model of the Arctic Ocean. *J. Offshore Mech. & Arctic Engrng.* **120**, 77–84.

Pritchard, R. S. 1975. An elastic-plastic constitutive law for sea ice. *J. Appl. Mech*. **43E** 379–84.

Pritchard, R. S., Coon, M. D. and McPhee, M. G. 1977. Simulation of sea ice dynamics during AIDJEX. *J. Pressure Vessel Technol*. **99J**, 491–7.

Proshutinsky, A. Y. and Johnson, M. 1997. Two circulation regimes of the wind-driven Arctic Ocean. *J. Geophys. Res*. **102**, 12 493–514.

Proshutinsky, A. Y., Polyakov, I. V. and Johnson, M. A. 1999. Climate states and variability of Arctic ice and water dynamics during 1946–1997. *Polar Res.* **18**, 135–42.

Rind, D., Healy, R., Parkinson, C. and Martinson, D. 1995. The role of sea ice in $2 \times CO_2$ climate model sensitivity. Part I: The total influence of sea ice thickness and extent. *J. Climate* **8**, 449–63,

Rothrock, D. A. 1975. The energetics of plastic deformation of pack ice by ridging, *J. Geophys. Res*. **80**, 4514–19.

Rothrock, D. A., Yu, Y. and Maykut, G. A. 1999. Thinning of Arctic sea-ice cover.
    Geophys. Res. Lett. **26**, 3469–72.
Schramm, J. L., Flato, G. M. and Curry, J. A. 2000. Toward modeling of enhanced basal
    melting in ridge keels. *J. Geophys. Res*. **105**, 14 081–92.
Schramm, J. L., Holland, M. M., Curry, J. A. and Ebert, E. E. 1997. Modeling the
    thermodynamics of a sea ice thickness distribution, 1. Sensitivity to ice thickness
    resolution. *J. Geophys. Res*. **102**, 23 079–91.
Semtner, A. J. Jr. 1976. A model for the thermodynamic growth of sea ice in numerical
    investigations of climate. *J. Phys. Oceanography* **6**, 379–89.
Shine, K. P. and Henderson-Sellers, A. 1985. The sensitivity of a thermodynamic sea ice
    model to changes in surface albedo parameterization. *J. Geophys. Res.* **90**, 2243–50.
Steele, M. and Flato, G. M. 2000. Sea ice growth melt and modeling: a survey. In Lewis,
    E. L. *et al.*, eds., *The Freshwater Budget of the Arctic Ocean*. Dordrecht, Kluwer,
    pp. 549–87.
Steele, M., Zhang, J., Rothrock, D. and Stern, H. 1997. The force balance of sea ice in a
    numerical model of the Arctic Ocean. *J. Geophys. Res*. **102**, 21 061–79.
Stössel, A., Lemke, P. and Owens, W. B. 1990. Coupled sea ice – mixed layer simulations
    for the Southern Ocean. *J. Geophys. Res*. **95**, 9539–55.
Thomas, D., Martin, S., Rothrock, D. and Steele, M. 1996. Assimilating satellite
    concentration data into an Arctic sea ice mass balance model, 1979–1985.
    J. Geophys. Res. **101**, 20 849–68.
Thorndike, A. S. 1987. A random discontinuous model of sea ice motion. *J. Geophys. Res.*
    92, 6515–30.
Thorndike, A. S., Rothrock, D. A., Maykut, G. A. and Colony, R. 1975. The thickness
    distribution of sea ice. *J. Geophys. Res*. **80**, 4501–13.
Tremblay, L.-B. and Mysak, L. A. 1997. Modeling sea ice as a granular material,
    including the dilatancy effect. *J. Phys. Oceanography* **27**, 2342–60.
Vinnikov, K. Y. *et al.* 1999. Global warming and northern hemisphere sea ice extent.
    Science **286**, 1934–7.
Wadhams, P. 1990. Evidence for thinning of the Arctic ice cover north of Greenland.
    Nature **345**, 795–7.
Walsh, J. E., Hibler, W. D. III and Ross, B. 1985. Numerical simulation of northern
    hemisphere sea ice variability, 1951–1980. *J. Geophys. Res*. **90**, 4847–65.
Zhang, J., Rothrock, D. and Steele, M. 2000. Recent changes in Arctic sea ice: the
    interplay between ice dynamics and thermodynamics. *J. Climate* **13**, 3099–114.